GUST LOAD ALLEVIATION BASED ON MODEL PREDICTIVE CONTROL

Hans-Gerd Giesseler[1], Michael Kopf[2,4], Timm Faulwasser[3], Paolo Varutti[4], and Rolf Findeisen[4]

[1]Airbus Operations GmbH Hamburg, Germany
hans.giesseler@airbus.com

[2]IBK-Technology GmbH & Co. KG, Germany
michael.kopf@ibk-tech.de

[3]Laboratoire d'Automatique,
Ecole Polytechnique Federale de Lausanne, Switzerland
timm.faulwasser@epfl.ch

[4]Laboratory for Systems Theory and Automatic Control,
Otto von Guericke Universität Magdeburg, Germany
{paolo.varutti, rolf.findeisen}@ovgu.de

Keywords: Gust Load Alleviation, Model Predictive Control, LIDAR

Abstract: Weight reduction is a typical design goal for modern aircraft. If gust encounters (as required by Certification Specification 25) are sizing conditions of parts of the airframe, this can be achieved (for example) by an active gust load alleviation system that reduces the gust load level down to the level of the next design condition, which might be the design loads from maneuver conditions. In order to design an efficient gust load alleviation system that respects the actuation constraints of the control surfaces, uses preview information on the incoming gust shape from a Light Detection And Ranging gust sensor and takes gust propagation delays into account, we apply model predictive control to an aeroservoelastic aircraft model.

GLOSSARY

AC ..... Aircraft	HTP .. Horizontal Tail Plane
CT ..... Continuous Turbulence	IQ ..... Interesting Quantities
CS ..... Control Surface	KF .... Kalman Filter
DistMod Disturbance Model	LIDAR Light Detection And Ranging
DG ..... Discrete Gust	MPC .. Model Predictive Control
FIM .... Fully Integrated Model	WRBM Wing Root Bending Moment
GLA ... Gust Load Alleviation	QP .... Quadratic Program

1 INTRODUCTION

Today's air traffic volume and its prospective growth, as well as the rising fuel costs and the ambitious targets for reduced emissions (COx, NOx, etc.), call for more eco-efficient aircraft. One important aspect of these objectives is the reduction of fuel consumption that intuitively can be achieved by decreasing airframe weight. In general, an aircraft (AC) is designed to withstand the flight loads (forces and moments) which act on the AC structure in response to externally applied forces (aerodynamics, inertia, thrust, etc.). These *design loads* are calculated according to the airworthiness regulations *CS-25* [1] in which various loading scenarios are defined. Among them are encounters of discrete gusts

(DG) and continuous turbulence (CT). Often these design conditions contribute to the loads envelope. For instance at the wing roots, they can define the strength of the structure and thereby translate into weight of the wing. The introduction of a suitable control scheme to actively reduce the loads at these stations in gust and turbulence encounter can result into weight savings without compromising safety. This would imply fuel savings and consequently a reduction of direct operating costs, making the AC more attractive for the customers.

As a suitable control scheme for the gust load reduction we propose model predictive control (MPC) [2–4]. MPC is an on-line optimization-based control strategy, successfully applied in process control since the 1970s. It is a structured approach which allows to consider multiple input multiple output systems, constraints on inputs, states and outputs, delays as well as linear and nonlinear system dynamics.
Here, we propose to use MPC to design an active gust load alleviation (GLA) system which takes measured or estimated gust information into account. The main idea of our approach is to reduce the distributed loads via minimizing interesting quantities (IQ). For the reduction of the distributed loads the wing root bending moment (WRBM) may be a valid indicator. We focus on the application aspects and the overall achievable results underlining the performance that can be achieved applying MPC based GLA schemes. A concise overview on GLA approaches as well as the control specific aspects of the proposed approach are presented in [5].

Our results are based on a full flexible AC model, which is reduced and time-discretized for the purpose of control design, cf. Section 2. The application of MPC to the GLA problem is discussed in Section 3. In Section 4 the DG and CT and the GLA parameters are defined. Simulation results for different gust types and different scenarios are presented in Section 5 and 6 and show the effectiveness of our approach in reducing the gust loads at relevant stations.

2 AIRCRAFT FULL FLEXIBLE MODELING

A fully integrated model (FIM) is used as a basis for simulations. The FIM is a time domain model that combines the large amplitude flight-mechanics with the small amplitude aeroelastics, see Figure 1. The point-wise unsteady airloads description in the frequency domain is represented in the time domain by using the Rogers' approach [6]. The formulation is with respect to body axis, which needs a modification of the aerodynamic matrices, see [7]. This provides the capability of simulating aeroservoelastic gust encounters in the time domain. Since this model is too complex for control purposes, it is only used for simulation, while a reduced version is provided for predictive control.

2.1 Brief Model Description

In general, the FIM can be understood as a set of ordinary differential equations with output equations

$$\dot{x} = f(x, u, g), \qquad y = h(x, u, g), \tag{1}$$

where x, y, u, g are the state, output, control and gust vectors, respectively. The effect of the vertical gust penetration is modeled by dividing the AC x-dimension into five sections. It is assumed that the gust velocity is recorded at the AC nose or ahead and acts at the

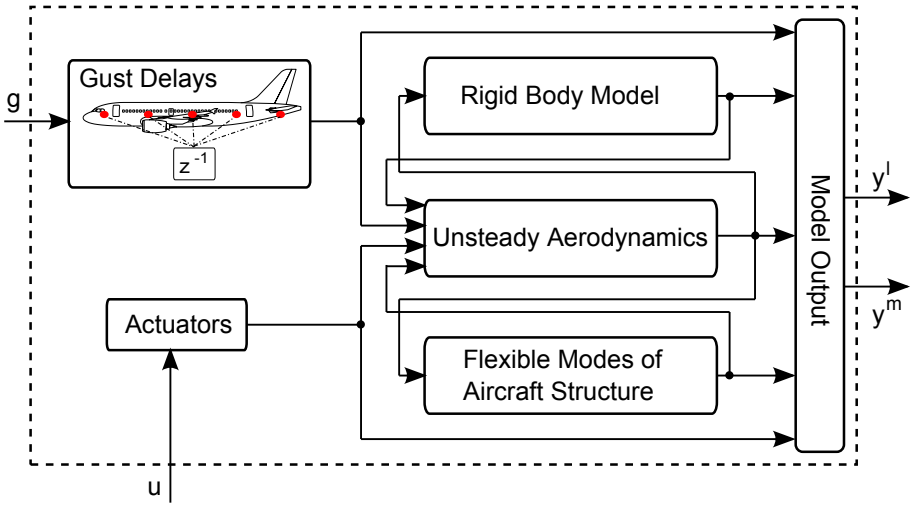

Figure 1: Fully integrated model, gust action delayed to red markers.

mid-point of each section and that the gust affects all panels belonging to one section at the same time.[1] The traveling delay of gust effects is modeled by a gust tab-vector $g = (g_1, \ldots, g_5)$, with $g_i = (v_{gi}, \dot{v}_{gi})$, where $v_{gi}(t) = v_g(t - \Delta x_i/V)$, with Δx_i the traveling distance from the point of gust measurement to the gust action point i, V is AC speed and $\dot{v}_{gi} = dv_{gi}/dt$. From this FIM model, we derived a reduced longitudinal model, linearized around 1g, for the purpose of controller design. This model contains only longitudinal motion parameters, i.e. rigid body states (forward and vertical speed, pitch rate and pitch attitude, generalized coordinates q_i)

$$x = (v_x, v_z, \omega_y, \vartheta, q_1, \ldots, \dot{q}_1, \ldots)^T . \tag{2}$$

The controls are grouped and applied symmetrically,

$$u = (DP_i, DP_m, DP_o, DSP_{1-3}, DSP_{4-6}, DSP_{7-8}, DQ_i, DQ_o)^T \tag{3}$$

where DQ, DP, DSP are elevator, aileron and spoiler. The subscripts i, m, o stand for inner, middle and outer, while the numbers refer to the corresponding grouped spoilers. The actuator stroke limitation translates into lower and upper deflection limitation $\underline{u}$, $\overline{u}$. The limitation of oil flow through the valves results in a maximum deflection rate $\dot{u}_{max}$ of the control surfaces.
The model output $y = \left(y^m, y^l\right)^T$ (1) contains several standard measurements

$$y^m = (V, \alpha, \omega_y, \vartheta, n_{cg}, n_i)^T , \tag{4}$$

where $V = |v|$ is AC speed, $\alpha = \arctan v_z/v_x$ is angle of attack, ω_y is pitch rate, ϑ is pitch angle, n_{cg} is local load factor at cg, and n_i is local load factor at some AC station (e.g. engines, fuselage, wing-tip, ...). This measurements are supplied to the flight control and guidance laws and/or cockpit display. The second virtual output contains other *interesting quantities* (IQ) for GLA that are usually not measured

$$y^l = (S_{wr},\ S_{wm1},\ S_{wm2},\ S_{hr},\ S_m)^T . \tag{5}$$

In detail these variables are: load at wing root S_{wr}, at two mid wing positions (S_{wm1}, S_{wm2}) and at the horizontal tail plane (HTP) root S_{hr}, see Figure 2. S_m are additional values

[1] Aerodynamic model may come from a panel method like *Doublet Lattice Method* [8].

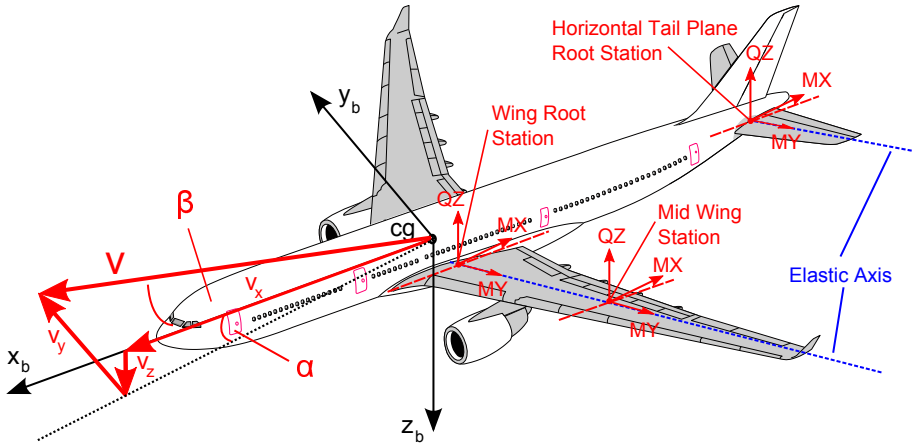

Figure 2: Loads relevant stations and measurable speed representation (polar, Cartesian coordinates).

of interest, e.g. lateral loads on engines, included into the output for monitoring at least. As we consider longitudinal (thus symmetric) motion, we can restrict the investigation to the right hand side stations. At station i, the loads $S_i = (Q_z, M_x, M_y)_i$ are shear, bending moment and torsional moment.[2]

For (1) a full flexible $1g$ trim solution (x_0, u_0, y_0, g_0), in the absence of gust $g_0 = 0$, is obtained from

$$0 = f(x_0, u_0, 0), \qquad y_0 = h(x_0, u_0, 0) \tag{6}$$

where some of the entries are specified while others are iterated to satisfy the equations. Taking the linearization w.r.t. the trim point, we obtain

$$\delta\dot{x} = A_c\delta x + B_c\delta u + E_c g, \qquad \delta y = C\delta x + D\delta u + Fg. \tag{7}$$

These equations are implemented in a MATLAB version of FIM/VARLOADS tool [7, 9, 10].

2.2 Reduced Model for Controller Design

Due to the high dimensionality of the model (7) (over 4000 states) and due to the large spread of modal frequencies, the linearized FIM (7) is not suitable for controller design. Thus a longitudinal model retaining the first five flexible modes with the control and output vectors as given in (3), (4) and (5) is derived. Furthermore, model reduction techniques are applied in three steps. First, all zero paths in the transfer function are canceled out. In a second step, the number of states are reduced by ensuring that observability is preserved. As this step does not retain the physical meaning of the state variables, the states which can be directly measured have to be included in the output vector. In a third reduction step, the number of states is further reduced to 24 states. The obtained model matches the original well for all frequencies of interest (up to $6Hz$). To improve the conditioning of the system and prevent numerical problems, the reduced AC model is finally balanced. The resulting longitudinal system is a state-space model with 27 outputs, 8 inputs, and 24 states.[3]

[2]Note that the wing weight is more sensitive to the WRBM M_x, less sensitive to shear force Q_z and torsional moment M_y.

[3]Note that for relevant changes in the design point (trim point), the controller design model must be updated, which includes execution of the model reduction steps.

Finally, the model is discretized with a sampling interval of $\Delta t = 0.02s$. This yields

$$x(k+1) = A \;\; x(k) + B \;\; u(k) + E \;\; g(k) \tag{8a}$$
$$y^m(k) = C^m x(k) + D^m u(k) + F^m g(k) \tag{8b}$$
$$y^l(k) = C^l \;\; x(k) + D^l \;\; u(k) + F^l \;\; g(k). \tag{8c}$$

This time-discretization is performed to facilitate the solution of the optimization problem appearing in the predictive controller, as explained in the preceding sections. Further details about the model reduction and discretization can be found in [11].

2.3 Output Scaling

To avoid numerical difficulties, which might occur from the differences in magnitude order of the measured outputs, the outputs (8b) and (8c) are scaled as

$$\widehat{y}_i = \frac{1}{y_{i_s}} \cdot y_i, \tag{9}$$

where y_{i_s} is the typical or acceptable range of the output y_i. For the measurable outputs y_i^m the scaling variable $y_{i_s}^m$ represents an acceptable deviation around the trimmed flight point. The scaling variable $y_{i_s}^l$ for the load outputs y_i^l is derived by

$$y_{i_s}^l = \theta \cdot \min_{y_{i_D}^l} \left(\left\| y_{i_D}^l - y_{i_0}^l \right\| \right), \qquad y_{i_D}^l = \left(y_{i_{\underline{D}}}^l, y_{i_{\overline{D}}}^l \right), \tag{10}$$

where $y_{i_{\underline{D}}}^l, y_{i_{\overline{D}}}^l$ is the lower and upper a-symmetrical design envelope. The trimmed loads $y_{i_0}^l$ (also called 1g-loads) are subtracted from the design loads to obtain the minimum distance to the design envelope. This minimum distance is multiplied by $\theta = 0.8$ to set the acceptable range of the loads to 80% of the minimum distance to the design envelope. The model (8), including the scaled outputs, is then used for predictive control.

3 MODEL PREDICTIVE CONTROL FOR GUST LOAD ALLEVIATION

MPC is a control method based on repeated online optimization. A cost function is optimized while taking into account system dynamics and constraints over a finite prediction horizon. From the resulting sequence of optimal control vectors, only the first vector is applied. The optimization is repeated at the next time step when a new measurement is available.Therefore MPC is often referred to as *moving horizon control* or *receding horizon control*. Current research has demonstrated the applicability of MPC to systems where the sampling intervals are in the millisecond-range. For more information and further background on MPC the reader is referred to [2, 4, 12, 13].

Key advantages of predictive control approaches for this application are: the use of available dynamic AC models, the direct consideration of actuator constraints as well as the consideration of a cost function for load reduction and also the possibility to include gust preview information.
The control problem of GLA can be formulated in terms of predictive control in the

following form:

$$\min_{u(i)} \quad \sum_{i=k}^{k+N_p} F\left(y^l(i), y^m(i), u(i)\right) \tag{11a}$$

subject to:

$$x(i+1) = Ax(i) + Bu(i) + Eg(i) \tag{11b}$$
$$y^m(i) = C^m x(i) + D^m u(i) + F^m g(i) \tag{11c}$$
$$y^l(i) = C^l x(i) + D^l u(i) + F^l g(i) \tag{11d}$$
$$u(i) \in \mathcal{U}, \quad \Delta u(i) \in \Delta\mathcal{U} \tag{11e}$$
$$x(k) = \hat{x}(k) \tag{11f}$$
$$u(k) = u^*(k|\hat{x}(k-1)) \tag{11g}$$

where (11a) represents the objective of reducing the loads on the airframe, (11b)-(11d) are the system dynamics and the output equations of (8). y^l is the load output which should be reduced while y^m is included to control the deviations of the rigid body state from the trim point. The constraints on the controls (11e) represent control surface deflection- and rate limits. At every time k, the optimization problem is solved and the optimal control sequence

$$U^*(k) = (u^*(k), u^*(k+1), u^*(k+2) \dots u^*(k+N_p))^T \tag{12}$$

is calculated. Only the first input $u^*(k)$ is applied to the system. And finally the optimization is repeated at the next time instant $k+1$ with a forward shifted horizon. In essence MPC is based on the repeated solution of the optimal control problem (11), whereby in each sampling step only the first control vector from (12) is applied. Note that in each sampling step the control is based on state information $x(k)$, i.e. MPC is a feedback control strategy. In this work, we use a Kalman filter (KF) to reconstruct the state $x(k)$ from the output measurements $y^m(k)$ (11c), see [14]. We refer to the estimated state at time k as $\hat{x}(k)$. It is based on the information provided by the measurements until time k.[4]

Picking the cost functional suitably is important to achieve stability as well as good overall performance. Staying close to the $1g$ trim point is a competing requirement to the GLA target of load reduction. Therefore the return to $1g$ after temporary deviation needs to be achieved by the MPC formulation. Hence, we minimize the incremental load output y^l without allowing too large deviations of the rigid body AC states from the trim point. In other words we penalize the available measurements y^m in the cost function F from (11). A quadratic cost function is a generic choice for many MPC problems. Here, we consider

$$F(y^l, y^m, u) = (y^l)^T Q^l y^l + (y^m)^T Q^m y^m + u^T R u, \tag{13}$$

which consists of three quadratic terms. The first term penalizes directly the loads while the second term is introduced for flight point stability. The third one accounts for the control inputs. The weighting matrices Q^l, Q^m, R are chosen such that $Q^l, Q^m \geq 0$ are positive semi-definite and $R > 0$ is positive definite. Note that we have only input constraints in (11) which ensures the existence of feasible solutions.

[4]Notice that an algebraic loop is generated due to the feed-through matrix D^m in (11c), see also [5]. In other words, to compute $\hat{x}(k)$, the KF needs to know $u(k)$ which results from solving the optimization problem for $\hat{x}(k)$ itself. To avoid this problem, we require that the first vector of the sequence (12) equals the second one (used in KF) of the previous input sequence, cf. (11g).

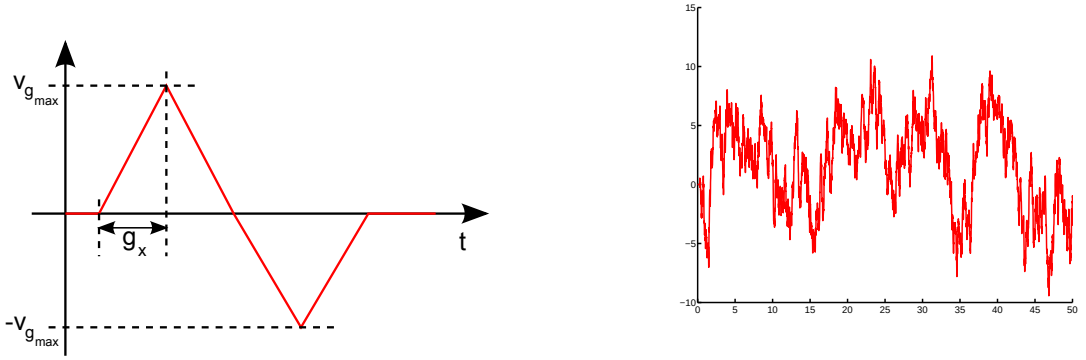

(a) Discrete gust type.

(b) Continuous turbulence gust type.

Figure 3: Considered gust types.

The optimal control problem (11) can be formulated as a quadratic program (QP). In other words, at each sampling instance we solve a QP using an open source QP solver [15].

4 SIMULATION SCENARIOS AND DEFINITIONS

4.1 Flight Point

Mainly, we want to reduce the loads at the wing root (because wing mass is susceptible to this IQ). Thus we consider the flight point known from loads design calculations to produce the extreme wing root bending. This flight point is characterized by cruise speed and an altitude of $h \approx 9000m$. The total AC mass (including fuel, cargo) is chosen to be close to the maximum takeoff weight. This choice provides a high WRBM for the trimmed $1g$ case, leaving less room for incremental dynamic-up bending.

4.2 Gust Types

We consider different gust encounter scenarios—parametrized DG and CT, cf. Table 1. The speed profile of the down/up discrete gust is shown in Figure 3(a). It is a gust doublet made of two triangular gusts with opposite sign. The down gust is given by the first triangle only. The *gust doublets* are beyond the *CS-25* [1] which requires only one-sided *1-cos* shapes which we approximate by the triangle gust shape. Parameters are the maximum gust speed and the gust gradient g_x, defined like in the *1-cos* case as distance from onset to first extrema. The continuous turbulence is very much like requested in *CS-25* [1] and parametrized in the same way by the standard deviation of the gust speed σ_g and by the turbulence length scale L_g.

key	Discrete Gust	key	Continuous Turbulence
(a)	up gust	**(e)**	Dryden Spectrum (CT)
(b)	down gust		
(c)	up/down gust		
(d)	down/up gust		

Table 1: Gust Types Considered

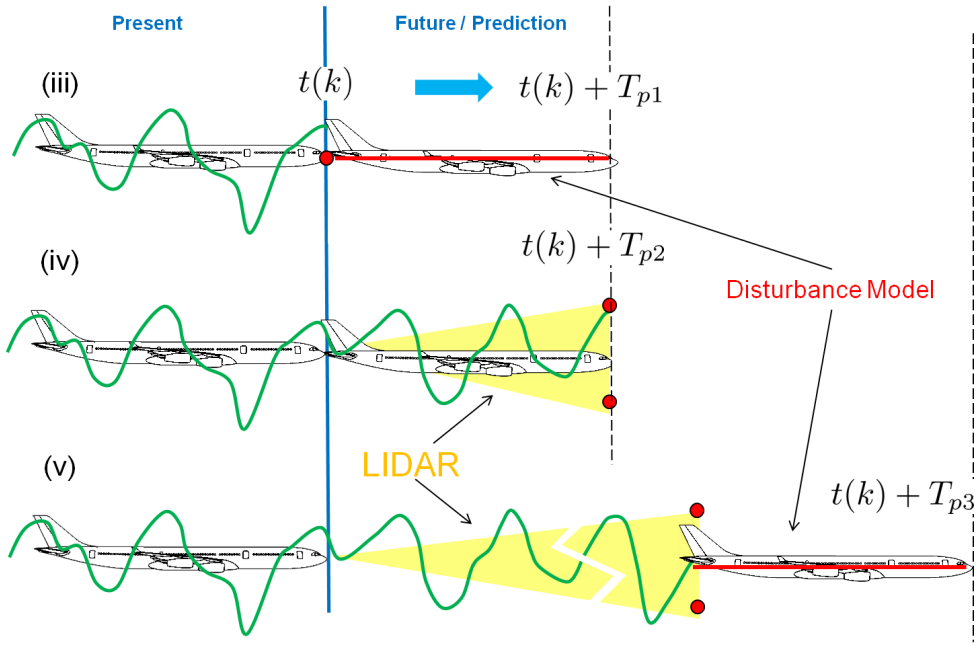

Figure 4: Prediction horizon due to nose and LIDAR measurements or disturbance model (DistMod).

4.3 GLA Assumptions

Five *control*-scenarios (i-v) are considered: natural AC (i.e. no control), reference GLA (ii) and GLA via MPC with three different prediction horizons (iii-v) based on different types of gust measurements and extrapolations. The considered measurement principles for the gust speed are:

- **Nose Measurement:** Local flow angles can be measured at AC nose, from which the gust angle of attack and sideslip can be obtained.
- **Measurement via LIDAR:** Installation of a LIDAR system allows to acquire gust speed information ahead of AC nose. The look ahead distance is $150m$, which is guaranteed for an ultraviolet LIDAR [16].
- **Disturbance Model:** If no LIDAR is available, we consider a disturbance model (DistMod) to provide the necessary information. Here we use as a DistMod the simple assumption of zero gust speed ahead of AC nose.

The basic idea is to include preview information as provided by LIDAR or DistMod in the MPC scheme to counteract disturbances before they arrive at the stations. For the three gust measurement principles, we consider the three scenarios (iii-v) depicted in Figure 4. Scenario (iii) shows an AC with nose gust sensor measurement (red circle) and the measured and stored gust shape at current time $t(k)$ (green line). The red part is ahead of the sensor measurement point and thus is still unknown. To consider the effect of the known green gust shape completely, the prediction interval T_p is chosen such that we can evaluate the stored gust information moving over the whole AC. For the AC parts that move into the red unknown gust shape zone where no information is available, we assume as a simple assumption a zero gust. In scenario (iv) we assume that we have a LIDAR installed, taking measurements ($64m$) ahead (at the red points). The prediction horizon is defined such that over the whole horizon the gust shape along the AC is known. In (v)

Simulation Key	GLA Type	CS	Measurement Type	Length (m)	T_p (s)
(i)	No GLA	0	-	-	-
(ii)	Ref. GLA	5	n_z at cg	-	-
(iii)	MPC	8	Nose+DistMod	$8+64$	0.26
(iv)	MPC	8	Nose+LIDAR	$8+64$	0.26
(v)	MPC	8	Nose+LIDAR+DistMod	$8+150+64$	0.82

Table 2: Parameters of considered GLA systems.

we extend scenario (iv) with LIDAR $150m$ range and gust set to zero for another $64m$ like in (iii), to provide an enlarged prediction horizon. We compare our results against the natural AC and against a *reference GLA*, which is defined to alleviate up-gusts only.[5]

All GLA systems compared during this simulation study are listed with their parameters in Table 2. The first column is the GLA scenario identifier. The control surface (CS) column denotes the number/set of CS used, which is $CS = 5$ for the reference GLA (no inner spoiler) and $CS = 8$ for the MPC based GLA (using also inner spoiler). The measurement type column refers to Figure 4 and the length column is the look-ahead distance for the gust measurement, which translates directly into the prediction horizon in terms of time T_p.

4.4 Comparison Criteria

In order to assess different scenarios, we define several comparison criteria. The aspects of static load reduction (i.e. the peak value) is reflected best by the maximum norm L_∞, applied to the time histories $y^i(k;u(\cdot))$.[6] The aspect of fatigue load reduction can be captured by the Euclidean L_2 norm. Two scenarios are compared by the ratio of these quantities

$$l^i_\infty = \frac{L_\infty(y^i_u)}{L_\infty(y^i_0)} = \frac{\max\limits_k |\, y^i(k;u(\cdot))\,|}{\max\limits_k |\, y^i(k;0)\,|}, \qquad l^i_2 = \frac{L_2(y^i_u)}{L_2(y^i_0)} = \frac{\sqrt{\sum_k (y^i(k;u(\cdot)))^2}}{\sqrt{\sum_k (y^i(k;0))^2}}, \tag{14}$$

with $k = 1, \cdots, N_{sim}$ and $i = 1, \cdots, q$. Here, N_{sim} is the number of simulation steps and q is the size of the output vector. We call these criteria *load modification factors in L_∞ and L_2 norm*, respectively. The GLA applications should also be compared to the upper and lower limit of the defined envelope. The maximum and minimum ratio $\overline{l^i_\infty}$ and $\underline{l^i_\infty}$ are defined as

$$\overline{l^i_\infty} = \frac{\max\limits_k y^i(k;u(\cdot))}{y^i_{\overline{D}}}, \qquad \underline{l^i_\infty} = \frac{\min\limits_k y^i(k;u(\cdot))}{y^i_{\underline{D}}} \tag{15}$$

[5]The main principle of this *reference GLA* is as follows: The cg-load factor is mapped into an auxiliary signal that is identical to the load factor as long as it increases. If the vertical load factor decreases, the last maximum is kept for, say, 5s. A nonlinear function converts this auxiliary signal into a deflection demand for ailerons and outer spoiler from which a compensatory pitch command for elevator is derived. The nonlinear function uses a threshold of 1.2g to command an aileron deflection demand and an increased threshold is to be crossed to involve the outer spoiler. This scheme breaks the direct link between load factor measurement and control surface deflection, which makes the law less vulnerable to failures of the sensor system and it makes the deflections less dynamic to guard against actuator wear. The up rigging of wing control surfaces leads to a down shift of the WRBM for a certain time span. Thus it might happen that the WRBM is increased due to an unexpected down gust. This is however not critical, since the design margins for down gust are typically larger than the ones for up gust.

[6]To simplify notation, we define $y^i_u := y^i(k;u(\cdot))$.

Output:	Description:	Output:	Description:
α_{AC} (rad)	angle of attack	Qz_wm2 (daN)	mid wing 2 shear force
ω_y (rad/s)	AC pitch rate	Mx_wm2 (daNm)	mid wing 2 bending moment
ϑ (rad)	AC pitch angle	My_wm2 (daNm)	mid wing 2 torsion moment
n_z (daN)	longitudinal load factor at cg	Qy_E1 (daN)	engine 1 lat. force in y-direction
Qz_wr (daN)	wing root shear force	Qy_E3 (daN)	engine 3 lat. force in y-direction
Mx_wr (daNm)	wing root bending moment	Qz_E1 (daN)	engine 1 vert. force in z-direction
My_wr (daNm)	wing root torsion moment	Qz_E3 (daN)	engine 3 vert. force in z-direction
Qz_wm1 (daN)	mid wing 1 shear force	Qz_hr (daN)	HTP root shear force
Mx_wm1 (daNm)	mid wing 1 bending moment	Mx_hr (daNm)	HTP root bending moment
My_wm1 (daNm)	mid wing 1 torsion moment	My_hr (daNm)	HTP root torsion moment

Table 3: Description of output entries in comparison tables.

where $y^i_{\overline{D}}$ ($y^i_{\underline{D}}$) is distance to upper (lower) limit. We denote these criteria as *margin factors for upper and lower envelope*, respectively.

The factors $(l^i_\infty, l^i_2, \overline{l^i_\infty}, \underline{l^i_\infty})$ allow to compare the different GLA scenarios. If their values are smaller than one, the GLA scheme is reducing the respective variable. We show these factors obtained from simulation studies in Tables 4 - 6. The IQs are shown in rows and the GLA scenarios in columns. The IQs or considered output variables are described in Table 3. The loads output subscripts (wr,wm1,wm2,E1,E3,hr) refer, respectively, to wing root, mid wing station 1 and 2, engine 1 and 3, and horizontal tail plane root.[7] In the following we refer to $(\alpha_{AC}, \omega_y, \vartheta)$ as the longitudinal rigid body AC states of interest. Note that the engine loads are not penalized in the cost function (11a) and are only listed here for monitoring.

4.5 Limits imposed by Airworthiness Requirements

The certification requirement *CS-25.302/Appendix K* [1] puts a limit on the active Gust Load reduction that static AC design can take advantage of. The loads calculated for a GLA in failure state, i.e. without GLA, must be sized with a Safety Factor of 1.0 while the loads in non-failed condition contribute to the sizing with a Safety Factor of 1.5. This means that a reduction of the *without GLA loads* by 1/1.5 is the maximum reduction that can become effective for static sizing. Alleviation margins lower than 2/3 can be used to compensate the current model uncertainties and simplifications in the MPC approach for GLA.[8]

5 ASSESSMENT OF GLA SYSTEMS FOR DISCRETE GUSTS

Subsequently, the control system behavior is analyzed using time history plots, for the severe gust parameter combination. The derived performance criteria for all scenarios are given in Table 4.

5.1 Severe Gust shape and Gradient

The WRBM response due to discrete gust types (a)-(d) from Table 1 is depicted in Figure 5(a) for a gust gradient $g_x = 100m$. This gust gradient yields the largest WRBM, see red solid line in Figure 7 showing the WRBM dependency on gust gradient. We see in

[7]Note that these are all right hand side loads, since for longitudinal motion the left and right hand

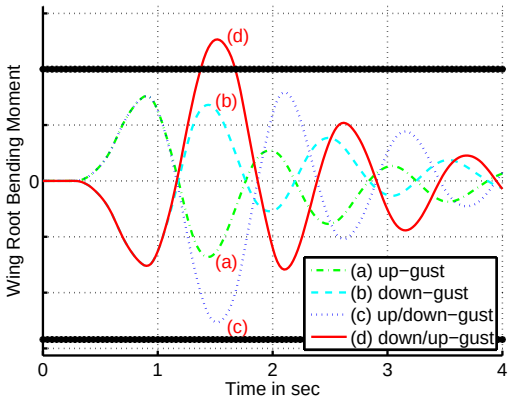

(a) Wing root bending for discrete gusts.

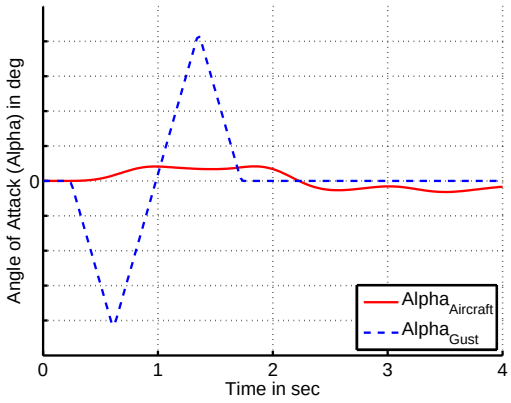

(b) Discrete down/up gust.

Figure 5: Analysis of discrete gust.

Figure 5(a) that the single triangle gust response (either up or down gust, symmetric w.r.t the 1g due to linear model) are not critical, as it stays away from the upper and lower envelope limit given by the black bold horizontal lines. The size of the WRBM second peak is similar to the first one, which suggests that it is due to inertia effects. For the up/down and down/up gust doublet, the second peak clearly exceeds the first one, which results from the inertia effects interfering with the gust sign reversal. The second peak of the down/up gust exceeds the upper limit. For the up/down gust the second peak is no problem, because of the larger distance to the lower envelope. There is a tendency that the AC response increases the effective angle of attack $\alpha_{eff} = (\alpha_{AC} + \alpha_{Gust})$ for the second gust peak, as it can be seen from Figure 5(b). However, this cannot explain the increase in the second peak, which is left to inertia loads. In order to alleviate the WRBM in gust encounter, we have in principle two possibilities which should be suitably combined: (I) destroy the disturbance effect directly at the wing via appropriate deflection of wing control surfaces or (II) reduce the effective angle of attack by pitching—via elevator—the AC into the gust. Deployment of wing controls for gust disturbance rejection is an obvious solution. However, it is not symmetric w.r.t. up and down gust. Spoilers can be used only to reduce up gust effects, since they are located on the upper wing surface and can be deflected upward only. Thus, in downward gusts it is mandatory (and it is as well recommended for the up gust) to take advantage of option (II): reduce α_{eff} by pitching the AC into the gust. This can also reduce the unfavorable superposition of inertial loads from a gust that already passed the wing and the aerodynamic loads of a newly arriving gust. Of course, using the elevator to pitch the AC has an effect on HTP loads and possibly on passengers comfort as well. The comfort effect can be easily accounted for, by introducing local vertical load factors increments $n_z(x)$ along the fuselage into the optimization problem (11).

We conclude that among the considered gust types the down-up gust shape (d) is the most critical discrete gust. Subsequently, we investigate the control parameters which play a role for alleviating this type of gust.

side loads are symmetric.

[8]For fatigue load reduction, there is no such limit.

5.2 Discussion of GLA Effect on Time Histories

For the down/up discrete gust discussed above, time histories of WRBM M_x (first subplot), effective angle of attack α_{eff} (second subplot) and the inner and outer elevator deflections (lower subplots) are shown in Figure 6(a), while wing controls are shown in Figure 6(b). In the second subplot of Figure 6(a), the gust speed at the wing is given by the black dashed curve.

By design, the reference GLA (ii) stays inactive for the first down gust part and becomes active only on the up gust part, see plot of wing controls (green dashed line). Some reduction in positive wing bending is observed. The MPC with nose measurement and assumed zero gust disturbance model (iii) reduces the WRBM for the down and up gust. However the reduction for the down gust is poor. Because of the short prediction horizon and also due to the disturbance model, there is no significant elevator deployment to pitch the AC into the gust to reduce the effective angle of attack. Very similar behavior can be observed for (iv). As depicted in Figure 4 the availability of full information over the short horizon does not improve the GLA performance for DG.

A significant improvement of the GLA performance is provided by GLA system (v) thanks to LIDAR $150m$ range and the additional zero gust assumption from the *disturbance model* for another $64m$ distance. This enables the appropriate α_{AC}-management that reduces already the down gust effect significantly and achieves overall a good WRBM reduction.

The control activity of the elevators are shown in the lower two subplots of Figure 6(a) for inner and outer elevator. The wing controls' activity are shown in Figure 6(b). Note that negative control surface deflections are always upwards. The green dashed curve (ii) reflects the activation logic of the reference GLA. There is an up deflection if load factor threshold is exceeded, keeping this value for a while if the load factor declines.

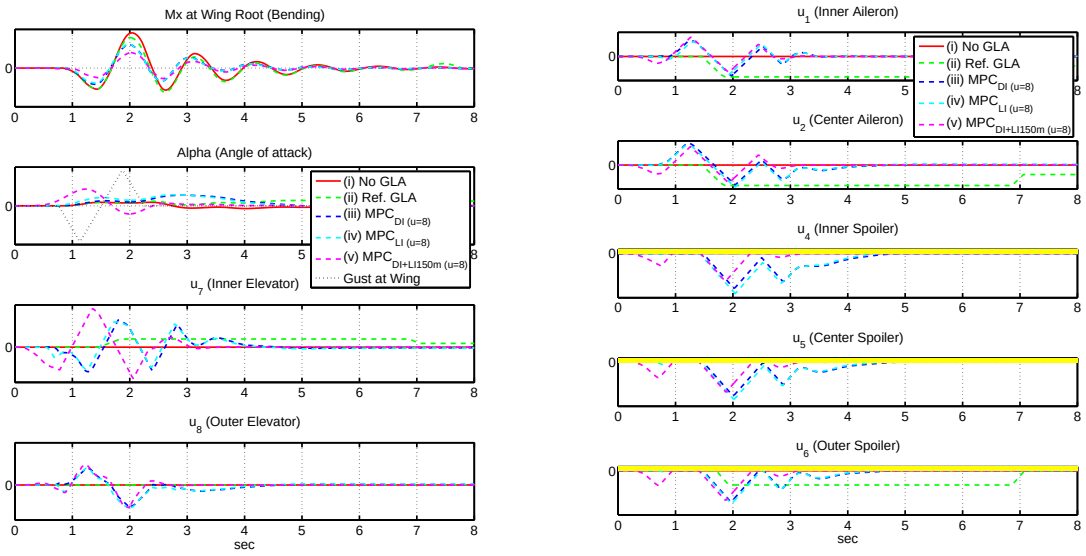

(a) Bending moment, angle of attack and elevators.

(b) Ailerons and spoilers.

Figure 6: Bending moment, angle of attack and controls for discrete down/up gust.

GLA Type:	(ii)	(iii)	(iv)	(v)	GLA Type:	(i)	(ii)	(iii)	(iv)	(v)
α_{AC}	**1.98**	**3.01**	**3.11**	**4.72**	α_{AC}	0.07	*0.14*	*0.22*	*0.23*	*0.34*
ω_y	**1.07**	**1.14**	**1.05**	**2.56**	ω_y	0.18	*0.19*	*0.20*	*0.19*	*0.31*
ϑ	**4.40**	**2.74**	**3.04**	**2.88**	ϑ	0.10	*0.45*	*0.28*	*0.31*	*0.30*
n_z	1.00	0.96	0.88	0.42	n_z	0.69	0.68	0.56	0.57	0.31
Qz_wr	0.97	0.69	0.75	0.49	Qz_wr	0.74	0.71	0.51	0.55	0.36
Mx_wr	0.87	0.67	0.68	0.44	Mx_wr	**1.27**	**1.10**	0.84	0.87	0.55
My_wr	**1.21**	**1.06**	**1.11**	0.66	My_wr	**1.17**	**1.41**	**1.24**	**1.29**	0.77
Qz_wm1	0.90	0.68	0.70	0.45	Qz_wm1	**1.17**	**1.06**	0.80	0.83	0.53
Mx_wm1	0.80	0.65	0.66	0.40	Mx_wm1	**1.48**	**1.19**	0.96	0.97	0.59
My_wm1	**1.32**	**1.04**	**1.02**	0.69	My_wm1	**1.46**	**1.92**	**1.47**	**1.49**	**1.00**
Qz_wm2	0.75	0.61	0.62	0.35	Qz_wm2	**1.34**	1.00	0.82	0.82	0.46
Mx_wm2	0.77	0.70	0.69	0.38	Mx_wm2	**1.05**	0.81	0.74	0.72	0.40
My_wm2	**1.50**	**1.52**	**1.35**	0.97	My_wm2	0.51	**1.03**	*0.67*	*0.72*	*0.53*
Qy_E1	**1.04**	0.87	0.88	0.59	Qy_E1	0.46	*0.48*	0.40	0.40	0.27
Qy_E3	**1.04**	0.74	0.72	0.47	Qy_E3	0.37	*0.38*	0.27	0.26	0.17
Qz_E1	0.96	0.64	0.82	0.73	Qz_E1	0.24	0.24	0.21	*0.28*	0.24
Qz_E3	**1.07**	0.96	0.99	0.73	Qz_E3	0.65	*0.69*	0.62	0.65	0.47
Qz_hr	**1.15**	**1.41**	**1.42**	**1.76**	Qz_hr	0.25	*0.37*	*0.46*	*0.46*	*0.57*
Mx_hr	**1.12**	0.81	0.75	**1.41**	Mx_hr	0.61	*0.68*	0.50	0.46	*0.86*
My_hr	0.78	**2.52**	**2.57**	**4.26**	My_hr	0.17	0.08	*0.42*	*0.43*	*0.71*

Table 4: GLA efficiency for DG: left: l_∞^i from (14), right: $\overline{l_\infty^i}$ from (15).

The GLA systems (iii, iv) show the activation shortly before the gust hits the wing; for inner elevators we see that (iv) commands slightly more pitch up initially, because of the perception of the gust sign reversal. A similar behavior is observed by GLA system (v), where the elevator activation starts a *long time* before the gust hits the wing, which provides the gust-opposing α_{AC} shown in the second rhs plot and also in the lhs plot for wing controls. It is interesting to note that there is a strong difference between inner and outer elevator for (iii) and (iv), which helps to minimize the horizontal tailplane wing bending. Obviously, most of the time the controls are rate-saturated. Thus a key performance bottleneck is the actuator rate limit.[9]

5.3 Comparison of GLA Performance for Discrete Gust

In the following we provide an overview over extreme outcomes for all IQs and for all scenarios (i-v). In the lhs part of Table 4 we compare the alleviation factor l_∞^i from (14) for different GLA implementations (ii-v). Values above unity are in bold and indicate an increase in peak value. In the rhs part of Table 4 the factor $\overline{l_\infty^i}$ from (15) compares the results against upper envelope (the critical side for wing). Variables with peak values above envelope are bold; if there is an increase w.r.t. natural AC the value is in cursive. From the lhs part of Table 4 we see that the reduction of the wing root bending by the GLA reference system (ii) is in the range of 13%. For the MPC system (iii-iv) we achieve a WRBM reduction of $\approx 32\%$.[10] For (v) we have a reduction of over 50%. Looking at other loads outputs, we see that some are increased due to the GLA activities. For all wing shear and bending loads, the MPC approaches (iii-v) decreases the load compared to the reference GLA system (ii). Note that an increased value (> 1) is not necessarily critical, as long as it can be covered by the envelope values (esp. the HTP loads). Finally, the MPC system (v) outperforms all other GLA approaches for discrete down-up gust, since all wing loads are efficiently reduced. The same holds for (lateral) engine loads. The increased values of the rigid body AC states ($\alpha_{AC}, \omega_y, \vartheta$) are due to the trade off between load reduction and trim point convergence. However, the load factor at the center of gravity n_z is reduced, which suggests an improved passenger comfort at least close to the

[9] We used $\pm 40^o/s$ which is a reasonable value for flight control, could be slightly increased for GLA applications, while staying within the performance limits of standard hydraulic devices.

[10] If we restrict MPC to use the same wing controls like (ii), which means no inner spoiler, the reduction for (iii-iv) is $26 - 28\%$.

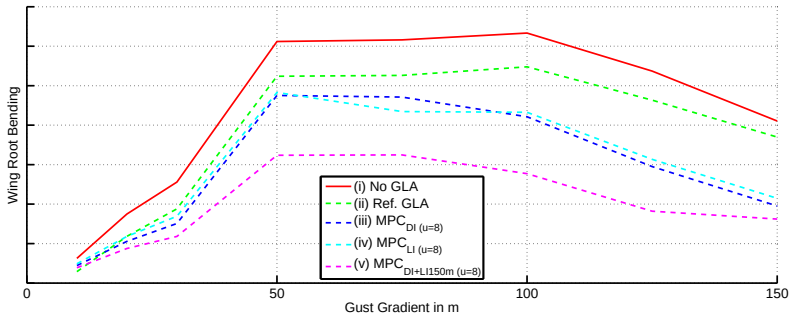

Figure 7: Wing root bending moment over gust gradient of discrete down-up gusts.

center of gravity.[11]

The rhs part of Table 4 indicates whether loads values that are increased by GLA action are likely to become critical. The table shows the criterion $\overline{l_\infty^i}$ from (15), since the upper envelope is the critical one. The wing root bending is reduced below envelope at all wing stations, however the wing torsion at root and at first mid wing station is still above the envelope for the MPC based GLA systems (iii) and (iv). With MPC (v) wing root torsion is well below envelope and torsion at first mid wing station is just at the envelope value. Thus the MPC system (v) with the large prediction horizon keeps the loads within the desired limits. We see that the HTP loads—although increased w.r.t. natural AC—are not critical at all.

5.4 Alleviation Effect over Range of Gust Gradients

Due to the airworthiness regulations a range of gust gradients $(10 - 150m)$ must be demonstrated, cf. *CS-25* [1]. Thus we investigate the alleviation potential for all these gust lengths. We perform a sweep over the requested gust gradient range. The WRBM over gust gradient is given in Figure 7 for the considered gust shape and GLA systems. For the natural AC (i) WRBM is maximal for the down/up gust with gradient $g_x = 100m$. All control laws achieve a reduction of peak WRBM for all gust gradients. The plots confirm that MPC schemes (iii-v) with all available control surfaces outperform the GLA reference system (ii). The GLA system (v) with enlarged prediction horizon yields an efficient reduction of the WRBM over the whole range of gust gradients. Furthermore, we observe that the percentage reduction is not uniform over the gust gradient. For example, for (v) it is slightly lower at a gust gradient of $50 - 75m$. GLA (v) activation shifts the maximum WRBM to occur now at a gust gradient of $g_x = 50 - 75m$.

6 ASSESSMENT OF GLA SYSTEMS FOR CONTINUOUS TURBULENCE

The continuous turbulence scenario as introduced in Section 4.2 may be another design driver for the WRBM. The CT parameters are defined in the airworthiness regulations *CS-25* [1], by specifying the standard deviation σ_g of the vertical gust speed and the turbulence scale length L_g. Both are parameters for the shaping filter design that yields a gust speed time history with a Dryden spectrum. In order to get statistically reliable results a Monte Carlo approach should be applied, which is beyond the scope of this

[11] Note that the local n_z along the fuselage needs to be monitored to judge on the passenger comfort elsewhere.

paper and subject of future work. Here, we utilize the available DG gust simulation and analysis environment by generating a CT sample of gust speeds which are deployed to the scenarios (i-v). From the sample we retrieve the most critical time slice, which is examined as a time history in more detail, and compared for the scenarios (i-v), see Figure 8. Thus—despite of the stochastic nature of the sample—we stick to the time histories. Therefore the CT investigation is similar to the DG case. The critical WRBM time slice is shown in Figure 8(a). Like for DG we show the two lhs and rhs set of subplots. One can see that the peak WRBM (red curve in lhs upper subplot) is reduced by all GLA systems. The effect of the reference system (ii) is to shift the load level downwards due to the constantly deflected ailerons (rhs plots). The GLA system (iii) reduces the peak WRBM. However, after the WRBM peak it exceeds the natural AC WRBM for a while, still remaining lower than the extreme WRBM from (i). This undesirable (but not critical) behavior is induced by an increased effective angle of attack α_{eff} due to AC response. The poor performance must be attributed to the simplicity of the disturbance model (iii) which assumes zero gust angle for the $64m$ horizon where—due to nose measurement—no data are available. This *zero gust speed extrapolated horizon* problem is avoided with (iv), where the extrapolation is filled with ($64m$ ahead of nose) LIDAR measurements. Consequently, GLA system (iv) leads to an evenly WRBM reduction over the whole time interval. This reduction is accompanied by reduced control surface activities and reduced peak deflections. The large prediction horizon (v), *LIDAR* $150m + 64m$ *DistMod* brings only slight improvements to the wing root bending but allows for different—and obviously more efficient—control usage compared to (iv). For (v) we observe less wing controls activity and a more dynamic use of inner elevator. GLA system (v) provides the smallest effective angel of attack, thanks to the elevator activity, enabled by the longer prediction horizon. In summary the system (v) uses (mainly inner) elevator to pitch the AC to reduce the imposed gust angle of attack.

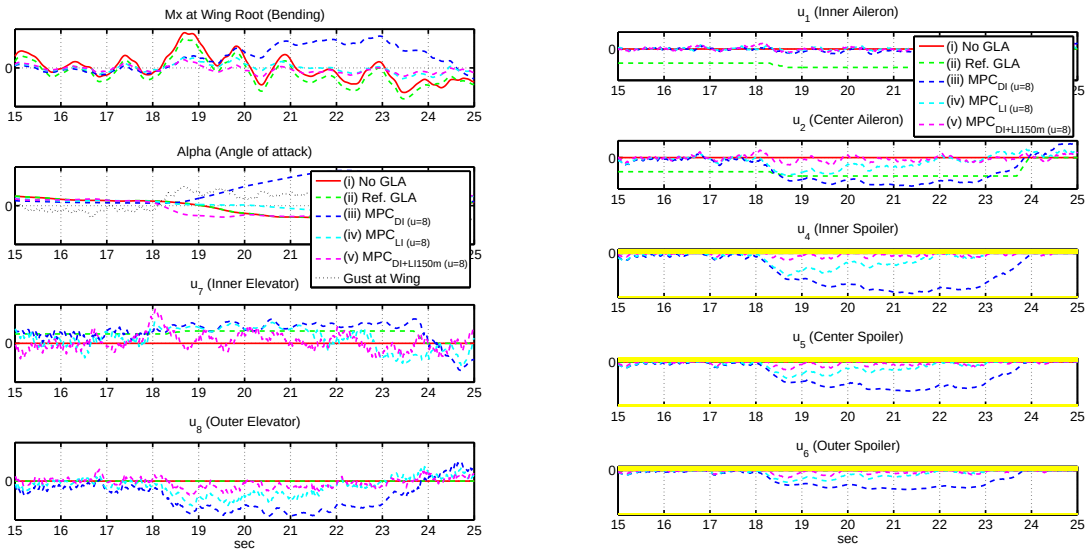

(a) Bending moment, angle of attack and elevators.

(b) Ailerons and spoilers.

Figure 8: Bending moment, angle of attack and controls for continuous turbulence.

GLA Type:	(ii)	(iii)	(iv)	(v)
α_{AC}	1.00	**1.75**	**1.02**	**1.11**
ω_y	**1.01**	**2.86**	0.94	**2.09**
ϑ	**1.25**	**7.85**	**1.53**	**3.41**
n_z	1.00	**1.41**	0.68	0.34
Qz_wr	0.96	0.90	0.61	0.39
Mx_wr	**1.06**	0.90	0.66	0.37
My_wr	**1.21**	**2.34**	**1.01**	0.53
Qz_wm1	**1.05**	0.91	0.71	0.40
Mx_wm1	**1.09**	**1.04**	0.58	0.30
My_wm1	**1.42**	**1.90**	**1.06**	0.62
Qz_wm2	**1.15**	**1.14**	0.47	0.31
Mx_wm2	**1.06**	**1.29**	0.47	0.30
My_wm2	**1.88**	**2.13**	**1.23**	0.71
Qy_E1	**1.04**	**1.54**	0.95	0.58
Qy_E3	**1.14**	0.95	0.59	0.62
Qz_E1	**1.02**	**1.10**	0.88	0.70
Qz_E3	**1.12**	0.92	0.83	0.72
Qz_hr	**1.45**	**2.51**	**1.16**	**1.19**
Mx_hr	**1.21**	**1.76**	0.59	0.95
My_hr	**1.28**	**4.09**	**2.22**	**2.37**

GLA Type:	(i)	(ii)	(iii)	(iv)	(v)
α_{AC}	0.40	0.40	*0.70*	*0.41*	*0.44*
ω_y	0.08	*0.08*	*0.25*	*0.08*	*0.19*
ϑ	0.17	*0.21*	**1.31**	*0.25*	*0.44*
n_z	0.43	*0.43*	*0.64*	0.23	0.15
Qz_wr	0.36	0.34	0.32	0.13	0.11
Mx_wr	0.47	0.39	0.42	0.14	0.15
My_wr	0.61	*0.74*	**1.44**	*0.62*	0.32
Qz_wm1	0.42	0.38	0.38	0.13	0.15
Mx_wm1	0.51	0.36	*0.53*	0.19	0.15
My_wm1	0.65	*0.93*	**1.23**	0.57	0.39
Qz_wm2	0.49	0.28	*0.55*	0.19	0.15
Mx_wm2	0.44	0.27	*0.56*	0.21	0.13
My_wm2	0.39	*0.78*	*0.89*	*0.40*	0.19
Qy_E1	0.21	*0.22*	*0.33*	0.17	0.12
Qy_E3	0.22	*0.26*	0.21	0.13	0.13
Qz_E1	0.43	*0.44*	*0.48*	0.38	0.31
Qz_E3	0.22	*0.24*	0.20	0.18	0.16
Qz_hr	0.20	*0.28*	*0.49*	*0.23*	*0.23*
Mx_hr	0.28	*0.34*	*0.50*	0.17	0.27
My_hr	0.09	0.04	*0.38*	*0.21*	*0.22*

Table 5: GLA efficiency for CT: left: l^i_∞ from (14), right: $\overline{l^i_\infty}$ from (15)

6.1 Comparison of GLA Performance in Continuous Turbulence

Like in the DG case, the CT results from the whole simulation are summarized in Tables 5 and 6 to provide a complete overview over GLA margins. As before we use the criteria from (14) and (15). From the lhs part of Table 5 we see that the reference system (ii) increases most of the loads output entries compared to natural AC. This may be acceptable, as the criteria does not distinguish between up and down loads increments. The MPC systems (iii) with disturbance model achieves a WRBM reduction of nearly 10%, whereas some other values are increased, especially wing torsion and HTP loads. Replacing the disturbance model by LIDAR measurement (iv), we recognize a strong wing bending reduction with a moderate increase in wing torsion. Like in the DG case, the MPC system (v) with the enlarged prediction horizon achieves the best WRBM reduction of 63%. Furthermore, all wing loads and also the load factor n_z at cg are significantly reduced too. As before, we compare the outputs with their upper envelope values to investigate whether increased values are critical or not. This comparison is shown in the rhs part of Table 5. GLA system (v) improves the margin w.r.t. the upper envelope on all wing stations. For the HTP there is an increase, but the load is around one third of envelope value. Thus when extrapolating the results to 3σ values (where we have to check that no control saturation occurs, to stay linear) we are still below the envelope.

For CT the L_2 norm is of interest, since it is relevant for fatigue design. This is depicted in

GLA Type:	(ii)	(iii)	(iv)	(v)
α_{AC}	**1.00**	**1.23**	0.96	**1.13**
ω_y	**1.00**	**2.48**	**1.01**	**2.06**
ϑ	**1.34**	**6.70**	**1.82**	**4.27**
n_z	**1.00**	**1.27**	0.57	0.32
Qz_wr	0.99	0.94	0.47	0.38
Mx_wr	**1.02**	0.80	0.41	0.33
My_wr	**1.12**	**1.91**	0.86	0.44
Qz_wm1	0.99	0.81	0.44	0.34
Mx_wm1	**1.10**	0.86	0.42	0.31
My_wm1	**1.41**	**1.72**	0.85	0.55
Qz_wm2	**1.26**	0.90	0.40	0.30
Mx_wm2	**1.24**	**1.06**	0.42	0.28
My_wm2	**2.38**	**2.15**	**1.00**	0.56
Qy_E1	**1.05**	**1.29**	0.64	0.44
Qy_E3	**1.05**	0.80	0.62	0.63
Qz_E1	**1.01**	0.79	0.71	0.54
Qz_E3	**1.09**	0.89	0.80	0.71
Qz_hr	**1.53**	**2.40**	**1.23**	**1.06**
Mx_hr	**1.15**	**1.38**	0.58	0.88
My_hr	**1.79**	**4.17**	**2.08**	**2.66**

Table 6: GLA efficiency for CT: Fatigue relevant l^i_2 criterion from (14)

Table 6. While (ii) increases the L_2-norm of nearly all loads outputs, the MPC based GLA provides a gradual improvement from (iii)-(v). With system (v) we provide significant reduction to wing loads with some penalty on HTP root loads. Thus, MPC using the LIDAR information has a clear loads reduction potential in DG and CT.

7 CONCLUSION

In this work, it was demonstrated how the problem of GLA for an aeroservoelastic aircraft can be solved by model predictive control. The proposed MPC scheme for GLA is based on recursive online solutions of quadratic programs. The *simulation model* used for performance demonstration was linearized around the trim point. For predictive controller design, the model order was reduced to yield a *design model*. The state for the *design model* was estimated using flight parameters and local load factor measurements.

Our investigations focused on discrete gust doublets—where down/up was found to be the most critical—and on flight in turbulence. The performance index accounts for controls, state and output quantities, the latter are the loads at relevant stations of the AC structure. Load alleviation performance improves with the anticipation capability for the incoming gust, which we assume to be measured by a LIDAR system. For the 150m look ahead LIDAR capability and the critical discrete down/up gust, wing root bending moment reduction was more than 50% with acceptable penalization on tail loads. If the LIDAR is not available on the AC, gust anticipation could be provided via improved disturbance modeling.

From our simulations it can be concluded that the maximum deflection limits are not critical for discrete gust. That is, the deflections computed by the MPC do not reach the limit values. However, the deflection rate limits are frequently attained. In other words, the GLA performance is limited by the imposed conventional deflection rate limits.

We have demonstrated that using the elevator to turn the AC into the gust is a significant contributor to the disturbance rejection element of the GLA system, which is naturally initiated by the proposed MPC control scheme.

Similar findings—not statistically rigorous—hold w.r.t. continuous turbulence encounter.

In future works we will investigate the effect of measurement errors and modeling uncertainties on the performance of MPC based GLA systems.

We can conclude that MPC provides a promising approach to GLA, which should be further investigated and extended towards loads optimal maneuvering in a gusty environment.

8 REFERENCES

[1] Joint aviation regulations - 25, airworthiness standards: Transport category airplanes. Vol. Subpart C - Structure.

[2] Findeisen, R. and Allgöwer, F. (2002). An introduction to nonlinear model predictive control. *21st Benelux Meeting on System and Control*, 119–141.

[3] Maciejowski, J. M. (2002). *Predictive Control*. Prentice Hall.

[4] Rawlings, J. and Mayne, D. (2009). *Model Predictive Control Theory and Design*. Nob Hill Publishing, Madison, WI.

[5] Giesseler, H.-G., Kopf, M., Varutti, P., et al. (2012). Model predictive control for gust load alleviation. In *Proc. 4th IFAC Nonlinear Model Predictive Control Conference (NMPC'12), Leeuwenhorst, Netherlands*. pp. 27–32.

[6] Roger, K. (1977). Airplane math modeling methods for active control design. *AGARD Structures and Materials Panel*, (AGARD/CP-228).

[7] Kier, T. and Looye, G. (2009). Unifying maneuver and gust loads analysis models. In *Proc. International Forum of Aeroelasticity and Structural Dynamics (IFASD), Seattle, USA (IFASD-2009-106)*.

[8] Rodden, W., Taylor, P., and McIntosh Jr, S. (September-October 1998). Further refinement of the subsonic doublet-lattice method. *Journal of Aircraft*, 35(5), 720–727.

[9] Scharpenberg, M., Kier, T., and Taules, L. (2011). Considerations on an integral flight physics model with application to loads analysis. *SAE International*.

[10] Hofstee, J., Kier, T., Cerulli, C., et al. (2003). A variable fully flexible dynamic response tool for special investigations (VARLOADS). In *Proc. 11th International Forum of Aeroelasticity and Structural Dynamics (IFASD), Amsterdam, Netherlands*.

[11] Kopf, M. (2012). *Performance Assessment of Model Predictive Control for Gust Load Alleviation*. Master's thesis, Otto-von-Guericke-University Magdeburg, Institute for Automation Engineering, System and Control Laboratory (Prof. Rolf Findeisen).

[12] Findeisen, R., Imsland, L., Allgöwer, F., et al. (2003). State and output feedback nonlinear model predictive control: An overview. *European Journal of Control*, 190–206.

[13] Mayne, D., Rawlings, J., Rao, C., et al. (2000). Constrained model predictive control: Stability and optimality. *Automatica*, 36(6), 789–814.

[14] Gelb, A. (1986). *Applied Optimal Estimation*. Massachusetts Institute of Technology Press, Cambridge, Massachusetts, and London, England.

[15] Ferreau, H. J. (2009). *qpOASES User's Manual*.

[16] Rabadan, G. J., Schmitt, N., Pistner, T., et al. (2010). Airborne LIDAR for automatic feedforward control of turbulent in-flight phenomena. *Journal of Aircraft*, 47(2), 392–403.